INTERNATIONAL JOURNAL OF CLIMATOLOGY
Int. J. Climatol. **19**: 931–950 (1999)

SEASONAL VARIABILITY OF THE GLOBAL OCEAN WIND AND WAVE CLIMATE

I.R. YOUNG*
Faculty of Engineering, Computer and Mathematical Sciences, University of Adelaide, Adelaide, SA 5005, Australia

Received 3 September 1998
Revised 5 January 1999
Accepted 21 January 1999

ABSTRACT

A data set spanning a period of 10 years and obtained from a combination of satellite remote sensing and model predictions is used to construct a global climatology of ocean wind and wave conditions. Results are presented for: significant wave height, peak and mean wave period and wave direction as well as wind speed and direction. The results are presented in terms of mean monthly statistics. The processed data set provides global resolution of 2°. The climatology clearly shows the zonal variation in both wind speed and wave height, with extreme conditions occurring at high latitudes. The important role played by the intense wave generation systems of the Southern Ocean is clear. Swell generated from storms in the Southern Ocean penetrates throughout the Indian, South Pacific and South Atlantic Oceans. During the Southern Hemisphere winter, this swell even penetrates into the North Pacific. The results confirm visual observations that the Southern Ocean is consistently the roughest ocean on earth. It is shown, however, that this is mainly caused by consistent high wind speeds, rather than the extended westerly fetch which exists. The west coasts of most continents have noticeably rougher wave climates than their respective east coasts, as a result of the longer generation fetches which exist on the west coasts. Copyright © 1999 Royal Meteorological Society.

KEY WORDS: world ocean; wave climatology; wind speed and direction; Southern Ocean; ocean waves and swell

1. INTRODUCTION

Numerous activities require accurate predictions of global ocean wave conditions. These activities span a range of traditional discipline areas and include geomorphological interests such as coastal shoreline stability and the seasonal longshore migration of sediment, engineering activities such as coastal and offshore structure design and operation, transport activities including optimal ship routeing and climate studies centred on air–sea interaction. Data for such activities have traditionally been obtained from three sources: *in situ* measurements using wave buoys, voluntary observing ship (VOS) data and the predictions of numerical models. Each of these data sources have limitations, particularly when global-scale climatology is required.

In situ measurements involve significant cost and typically span relatively short durations. Hence, a reliable assessment of seasonal variability is typically difficult to obtain. They do, however, provide the potential for high quality information at specific locations. Even extensive systems, such as the US NDBC network, however, cannot provide global or even basin-scale climatology. Such systems are, however, essential for calibration and validation of other data gathering techniques (Cotton and Carter, 1994; Sterl *et al.*, 1998; Young, 1998).

Voluntary observing ship data (Gulev *et al.*, 1998) provide the opportunity for global-scale observations of wave conditions. The data are, however, spatially inhomogeneous, confined to major shipping routes. Thus, areas such as the Southern and South Pacific Oceans have little available data. In addition, shipping

* Correspondence to: Faculty of Engineering, Computer and Mathematical Sciences, University of Adelaide, Adelaide, SA 5005, Australia; e-mail: iyoung@eng.adelaide.edu.au

CCC 0899–8418/99/090931–20$17.50

naturally attempts to avoid extreme weather conditions and hence high sea states may be under represented in the data set. Because such observations are visual, the accuracy of the data may also be inferior to other sources. Despite these limitations, VOS data have been used to compile global wave statistics (Hogben and Lumb, 1967; Hogben *et al*., 1986).

Numerical models provide a cost-effective means for the acquisition of global-scale data. They are, however, limited by the adequacy of the underlying model physics and the accuracy of input wind fields used to drive the models (Komen *et al*., 1994). Recently, however, global climatology based on long-term model hindcasts has been presented (Sterl *et al*., 1998).

The advent of satellite remote sensing systems provides the opportunity to obtain truly global data on oceanic wind and wave conditions. Some initial attempts have been made to obtain global wave climatologies from such data (Young, 1994; Young and Holland, 1996). These studies have been limited by the relatively short temporal period for which data were available (3 years) and the fact that only the significant wave height, H_s and wind speed, U_{10} were considered. Parameters such as the wave period and wave propagation directions were not available.

A number of satellite instruments are available for the determination of wave height and wind speed and direction. These instruments include: the Special Sensor Microwave Imager (SSMI); the Synthetic Aperture Radar (SAR); the Scatterometer and the Radar Altimeter. SSMI instruments have operated on a number of satellite platforms dating from 1987. They provide measurements of wind speed at a resolution of 29×37 km and with a relatively low accuracy of about 8 m s^{-1} (Hollinger, 1991). Scatterometers have flown on both ERS1 and ERS2 and provide measurements of both wind speed and direction. As such, the scatterometer has become the instrument of choice for satellite-based wind field measurements. The processing of scatterometer data are however, relatively involved and the routine determination of global data is still not available. The SAR offers the potential for the determination of the full wave spectrum (Hasselmann *et al*., 1996). The nonlinear mapping associated with the SAR transfer function has, however, posed a significant practical difficulty and routine SAR-based wave spectral data are not yet available. In addition, the power requirements of the instrument limits the global coverage. Radar altimeters have operated routinely on a number of satellites since 1986. The altimeter can measure wave height to an accuracy of $\pm 10\%$ and wind speed to an accuracy of $\pm 15\%$ (Young, 1998). The long data record, together with the relatively high spatial resolution of the instrument (≈ 10 km) and the ease of data processing, makes the altimeter ideal for large-scale wind and wave climate studies. For these reasons, it has been adopted in the present study.

Unfortunately, not all of the desired characteristics of the ocean wind and wave fields can be obtained from altimeter data. Examples are the wave period and the mean wind and wave directions. Highly sophisticated global wave prediction models have also been operational for a similar period, the sophistication and reliability of such models progressively improving over this period. Therefore, it is feasible to construct a comprehensive global database from a combination of satellite and model-derived data.

This paper presents such a database of global wind and wave quantities. The database includes values of: the significant wave height, H_s, the mean and peak wave periods, T_m and T_p, respectively, the wind speed, U_{10} and the mean wind and wave directions, θ_u and θ_w, respectively. Although the data base provides global climatology for both winds and waves, the primary focus of the paper is on the global wave field. The database is used to investigate the seasonal variability of the global wave field and to assess and explain numerous features of the wave climate in various regions. The global wind field represents an essential element in understanding the physical processes responsible for the wave climatology. For convenience of presentation, data are presented in the form of mean monthly values.

The arrangement of the paper is as follows. Section 2 presents the various data sources (instruments) which have been used to construct the database including an assessment of their accuracy and Section 3 details the techniques used to process these large data sets to form the present database. The results, as they apply to the global wave climate are presented in Sections 4 and 5. Section 4 presents results showing the seasonal variability of global wave parameters. The impact on various regional areas is presented in Section 5 with an analysis of the factors which control the wave climate in these regions. Finally, Section 6 presents conclusions and the assessment for future development of such database systems.

2. DATA SOURCES

Two general data sources have been used to construct the database: satellite measurements and model results. It would be desirable to rely completely on measured data and not utilise model results. In principal this is possible, as all of the required quantities can be measured by satellite. In practice, however, the reliability or the length of time for which a particular data set is available limits the use of some data. The available data sources are outlined below.

2.1. Significant wave height

The Radar Altimeter has been widely adopted as a highly reliable instrument for the measurement of the significant wave height, H_s (H_s is defined here in terms of the variance of the wave record, m_o as $H_s = 4\sqrt{m_o}$). The details of the theory by which the altimeter determines H_s have been summarised by Dobson and Monaldo (1996). The accuracy of individual measures is generally stated as $\pm 10\%$ or 0.5 m, whichever is the greater. Detailed calibrations of the instruments on a number of satellites by Cotton and Carter (1994) and Young (1998) indicate that such estimates of the accuracy are conservative.
Altimeters have been carried on a number of satellite missions, including:

(i) GEOSAT: November 1986–January 1990
(ii) TOPEX: September 1992–present
(iii) ERS 1: August 1991–present
(iv) ERS2: May 1995–present

For the present paper, data from GEOSAT, TOPEX and ERS1 have been used for the period up to October 1995. The raw H_s products from each of the satellites were corrected using the calibration results developed by Young (1998). The Young (1998) result is consistent with, but extends, the correction proposed by Cotton and Carter (1994). Hence, ≈ 10 years is spanned by the data set.

2.2. Wave period

The Synthetic Aperture Radar (Alpers and Rufenach, 1979; Alpers *et al*., 1981; Raney, 1981; Alpers, 1983; Hasselmann *et al*., 1985; Alpers and Brüning, 1986) can measure the directional wave spectrum from which quantities such as the wave period and mean wave direction can be obtained. Such instruments have been carried on both ERS1 and ERS2. The transfer function relating the SAR image spectrum to the wave spectrum is still a matter of some debate, although recent results are promising (Hasselmann *et al*., 1996). In addition, processing of SAR data is an involved task and long-term global usage may not yet be feasible. For these reasons, this data source has not been utilised for the present application. Rather, model results from the third generation spectral wave model WAM have been used (Komen *et al*., 1994). This model has been widely adopted by the international community and has been validated on numerous occasions (Janssen *et al*., 1996). These validation exercises reveal the model to be remarkably reliable. In the present context, it has been used to obtain two measures of the wave period, T_p and T_m. The peak wave period, T_p is defined as the peak ordinate of the spectrum. In cases where there is a mixture of swell and wind sea, the parameter can be noisy. Generally, however, T_p is a reliable measure of the longer period waves. It provides a good estimate of the period of swell in a particular area. In contrast, the mean wave period, T_m is an integrated weighted mean over the full spectrum. Values of T_m tend to reflect the locally generated wind sea. For the present application, these quantities have been taken from the global implementation of the WAM model which is operational at the European Centre for Medium Range Weather Forecasting (ECMWF). Data from the 5-year period June, 1992–May, 1996 were used for the present study. The standard operational ECMWF data products '231' for T_p and '232' for T_m were used. During the first 2 years of the data period, the model was run at a 3° resolution, a higher 1.5° resolution being used in later years. A consistent 3° data set was obtained by decimating all 1.5° resolution data to this coarser level. This data period was selected as it overlapped the period for which altimeter data were available, thus creating a consistent composite data set. Longer and higher resolution WAM data sets (Sterl *et al.*, 1998) have subsequently been produced. Whether such data sets would significantly enhance the resulting global climatology is yet to be determined.

2.3. Wind speed

The Radar Altimeter can also measure the wind speed, U_{10}, although with less accuracy than for H_s. The wind speed is obtained indirectly from the backscatter radar cross-section σ. The relationship between σ and U_{10} has generally been determined empirically from comparison with buoy data. A large number of relationships have been proposed, including Chelton and Wentz (1986), Witter and Chelton (1991) and Young (1993). In a recent validation, Young (1998) has shown consistently reliable results from GEOSAT, TOPEX and ERS1 altimeters with an accuracy of $\approx \pm 15\%$. For consistency, data from the same period and satellites as indicated for H_s have been used here. The calibration corrections proposed by Young (1998) were applied to the present data.

2.4. Wind and wave direction

As indicated above, wave direction can be measured using satellite-based SAR. For the reasons outlined above (with regard to wave period), this is not feasible for the present application. For this reason, the ECMWF global wave model (WAM) has also been used to obtain the mean wave direction, θ_w. The same data period and resolution as used for wave period have again been adopted for θ_w, but being obtained from the ECMWF operational product '230'.

Wind direction, θ_u, can be measured with Scatterometers such as those carried on ERS1 and ERS2. Difficulties with processing a long-term global data set and interpretation of the 180° directional ambiguity in such data makes it impractical for the present application. Again, model data have been used. The ECMWF global atmospheric circulation model has been utilised for this purpose with data spanning the period January 1985–December 1990 being used. ECMWF re-analysis level III-B global atmospheric data were used with θ_u being obtained from the surface level data. The model was run at 1.125° resolution, but the data was obtained and processed at a reduced 2.5° resolution.

3. DATA PROCESSING

3.1. Satellite altimeter data

Altimeter data are far from error free. Erroneous data occur for a number of reasons, typical examples being data spikes at the continental boundaries or where islands or exposed reefs fall within the altimeter footprint. Although such errors are obvious on visual inspection, manual quality control is clearly not feasible with such a large data set. A two-pass automatic data-checking algorithm was implemented with the following steps.

3.1.1. Pass 1.

(i) The satellite-derived values of H_s and U_{10} are the average of a number of individual radar pulses. The number of pulses varies between 10 and 20 depending on the particular satellite. Averaging of these pulses is performed onboard the respective satellite. The mean values (H_s or U_{10}), together with the standard deviation of the individual radar pulses, (σ_H, σ_U) are transmitted to the ground station. If σ_H/H_s or σ_U/U_{10} were greater than 0.1, the observations were discarded as there was obviously significant spatial variability.

(ii) A 1/12° land mask was used to determine the position of land masses. Any data corresponding to land, according to the mask, were discarded.

(iii) Only values of H_s in the range 0–20 m and U_{10} in the range 0–40 m s^{-1} were retained.

3.1.2. Pass 2.

(i) The remaining data were divided into blocks of 50 points, ensuring these passes had no spatial 'jumps' corresponding to the passage of the satellite over a continent. The mean values $\bar{H}_s$ and $\bar{U}_{10}$ and the standard deviations σ'_{H} and σ'_{U} of the 50 points in the block were determined. If $\sigma'_{\mathrm{H}}/\bar{H}_s > 0.5$ or $\sigma'_{\mathrm{U}}/\bar{U}_{10} > 0.5$, the respective values of the entire 50-point block were discarded as it obviously contained multiple data outliers.
(ii) Individual data outliers within the blocks were rejected using the criteria: $|H_{\mathrm{s}} - \bar{H}_{\mathrm{s}}|/\sigma'_{\mathrm{H}} > 3$ and $|U_{10} - \bar{U}_{10}|/\sigma'_{\mathrm{U}} > 3$.

Data from an extensive number of satellite passes were visually examined. Based on this visual inspection, it was concluded that the technique was capable of yielding data, free of erroneous values. Close to continental land masses the process was probably conservative, rejecting some valid data. In the present context, where interest is focused on global-scale data, this is of little consequence. Should interest be focused in coastal regions, a more refined technique would be required.

3.2. Model data

Processing of the model data was far more straight forward. Model predictions were obtained for 12 h GMT at each model grid point for the full 5-year model data set. These values were assumed representative of the respective model grid squares and averaged to yield monthly values. In the case of θ_{u} and θ_{w}, vector averages were performed.

4. GLOBAL VARIATION OF WAVE CONDITIONS

A number of previous investigators have used radar altimeter data to investigate global values of H_{s} and U_{10}. Chelton *et al.* (1981) produced a global 3-month average H_{s} field from the relatively short data set available from the SEASAT mission. Mognard *et al.* (1983) used this same data set to produce mean monthly H_{s} fields for the Southern Hemisphere winter of 1978. Challenor *et al.* (1990), Carter *et al.* (1991), Romeiser (1993) and Young (1994) used GEOSAT data to investigate global variations in H_{s}. Young and Holland (1996) used a combination of GEOSAT altimeter data and atmospheric circulation model results to investigate global mean monthly H_{s}, U_{10} and θ_{u} fields.

The present application extends both the number of quantities for which data are available and also the period over which the data set has been obtained (≈ 10 years). The satellite data were partitioned into $2° \times 2°$ sampling squares on the Earth's surface. The satellites return approximately one measurement each of H_{s} and U_{10} every second. Hence, the typical passage of a satellite through a sampling square returned ≈ 150 observations of each quantity. During the 10-year span of the composite GEOSAT, TOPEX and ERS1 satellites each sampling square was subjected to an average of 750 satellite passes. Consequently, there was a total of ≈ 110000 observations of each of H_{s} and U_{10} for each sampling square.

The model results were available on a $3° \times 3°$ grid with data being obtained at 12-hourly intervals. Hence, there was a total of ≈ 3600 observations of each of the model quantities (T_{p}, T_{m}, θ_{w}, θ_{u}) for each sampling square during the 5-year period for which model data were available.

The selection of the size of the sampling squares was a compromise between obtaining high resolution and sufficient data to obtain reliable statistics. The data partitioning adopted here provides both high resolution and greater data density than previously utilised. These previous studies indicate that the scheme adopted above should provide reliable results with a resolution not previously possible (Tournadre and Ezraty, 1990; Young, 1994, 1998).

The gridded data were processed to yield mean monthly values which are shown in Figure 1(a)–(f). These figures show shaded isopleth plots of mean monthly values of each of the quantities (H_{s}, U_{10}, T_{p}, T_{m}, θ_{w}, θ_{u}) Results are shown for the months of January, April. July and October, representing each of the four seasons. Space limitation preclude the display of the full 12-month sequence for each quantity.

Numerous features of the global wave climate are apparent in Figure 1(a)–(f). A number of the more important features are discussed below.

4.1. Zonal (latitude) variations

The most striking feature of the global distribution of H_s (Figure 1(a)) is the zonal variation. The highest wave conditions are seen at the higher latitudes. This is particularly clear in the Southern Ocean where intense wave conditions are observed year round, although they peak during the Southern Hemisphere winter (July–August). A similar situation exists in the Northern Hemisphere with peak conditions again occurring during winter (January) in both the North Pacific and North Atlantic Oceans. Although the peak values are similar in both hemispheres, the seasonal variabilities contrast dramatically. The maximum values of H_s occur in the Southern Ocean region between South Africa and Australia, where conditions peak at $H_s = 5.4$ m during August. Maximum condition in the Northern Hemisphere occur in the North Atlantic, where a maximum mean monthly value of $H_s = 5.2$ m occurs in January. At these same locations, the summer values are 3.66 m (Southern) and 2.53 m (Northern). Hence, although the maximum values are similar, the seasonal variability in the Northern Hemisphere is much greater than

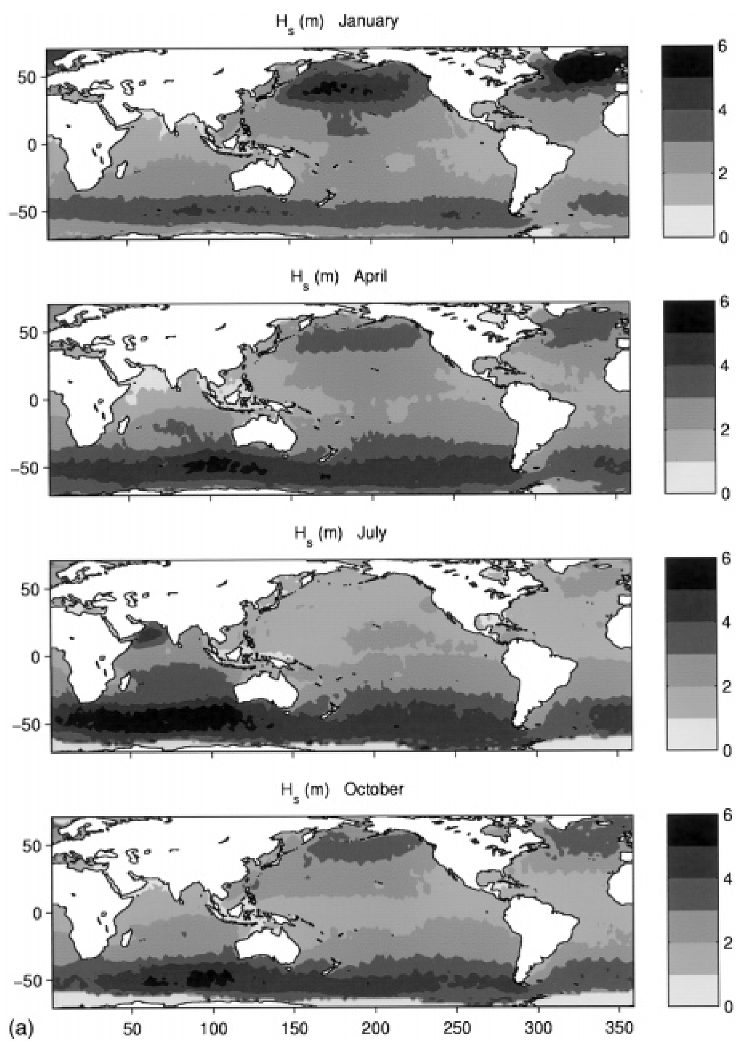

Figure 1(a). Global distributions of mean monthly values of the significant wave height, H_s for the months of January, April, July and October. Values are shown in units of meters as defined by the colour bar to the right

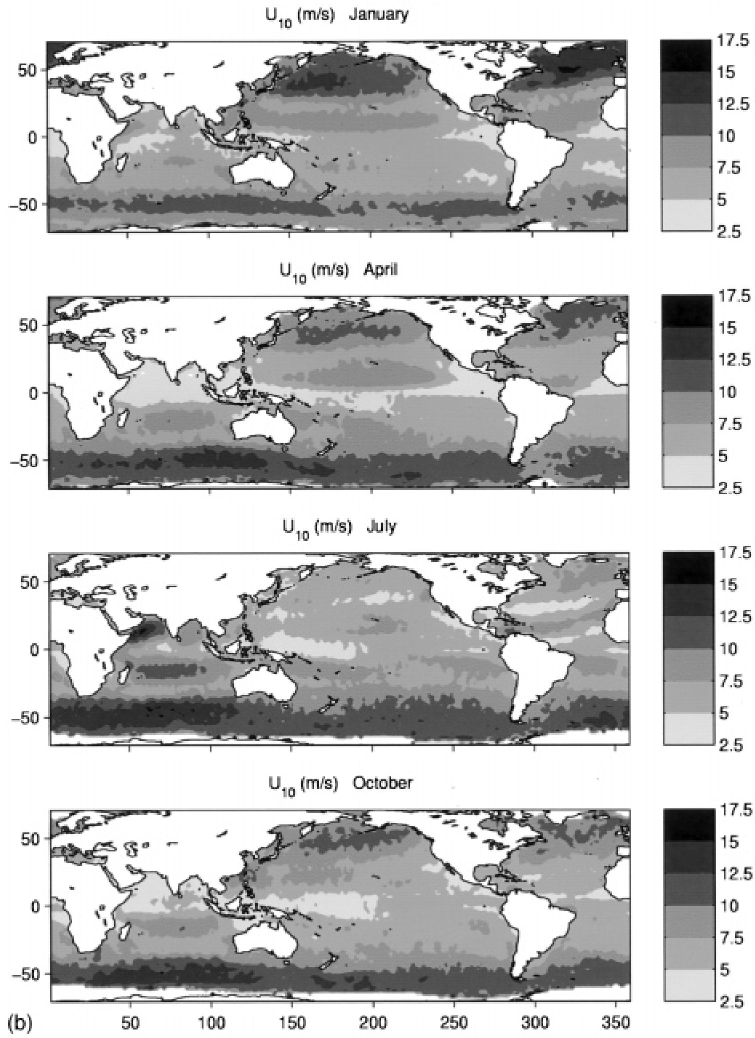

Figure 1(b). Global distributions of mean monthly values of the wind speed, U_{10} for the months of January, April, July and October. Values are shown in units of meters per second as defined by the colour bar to the right

in the Southern Hemisphere. The reputation of the Southern Ocean as being rough year round is well founded.

It is often assumed that the high wave conditions which occur in the Southern Ocean occur as a result of the extended fetch provided for westerly winds. This is the only region of the globe where there is no interruption by land in the east–west direction. Although the long fetches play a role, Figure 1(b) indicates that high wind speeds are more important. The wind speed (U_{10}) variations at these high latitudes largely follow the same seasonal trends observed for H_s. At the same North Atlantic location considered above, U_{10} varies from 15.1 to 7.9 m s^{-1} between winter and summer, whereas in the Southern Ocean the variation is from 15.0 to 10.2 m s^{-1}. Therefore, as noted for H_s, the maximum values of U_{10} (winter) in both hemispheres are similar. The Northern Hemisphere, however, experiences much lower winds in summer than does the Southern Hemisphere. Therefore, at these latitudes the wind speed seems to play a more significant role in determining the wave height than does the fetch. It can be concluded that the fetches in both hemispheres are sufficiently large that other influences, such as the magnitude and duration for which winds are sustained by a storm, are more important in determining the maximum waves generated. Hence, the waves appear to be limited by the maximum wind speeds and the duration of the storms rather than the fetch.

In contrast to high latitudes, equatorial regions are calm all year round, with little seasonal variability. The global wave fields show a progressive decrease in H_s from high latitudes to the equator. The wind fields, however, show a local increase in the subtropical regions associated with the trade-wind belts (e.g. $\pm 20°$ in Figure 1(b)). These local maxima do not occur in the wave fields, because waves are not purely local. Once generated, they propagate away from the generation region in the form of swell. The net result is that the wave height field varies far more smoothly than does the wind speed.

4.2. West coast wave climates

The western coasts of the continental land masses (particularly in the Southern Hemisphere), have a consistently rougher wave climate than their respective east coasts. This is particularly clear for both Australia and South America. At the latitudes of these land masses, the mean wind and wave directions (Figures 1(f) and 1(e)) are from the west. Therefore, the west coasts experience long fetches and hence higher wave climates. In addition, the wind speed to the east of South America appears to be consistently lower than to the west (Figure 1(b)). This is presumably a result of the blocking effect of the Andes Mountains. The clear reduction in wave climate caused by the relatively narrow Drake Passage to the south of South America is also clear.

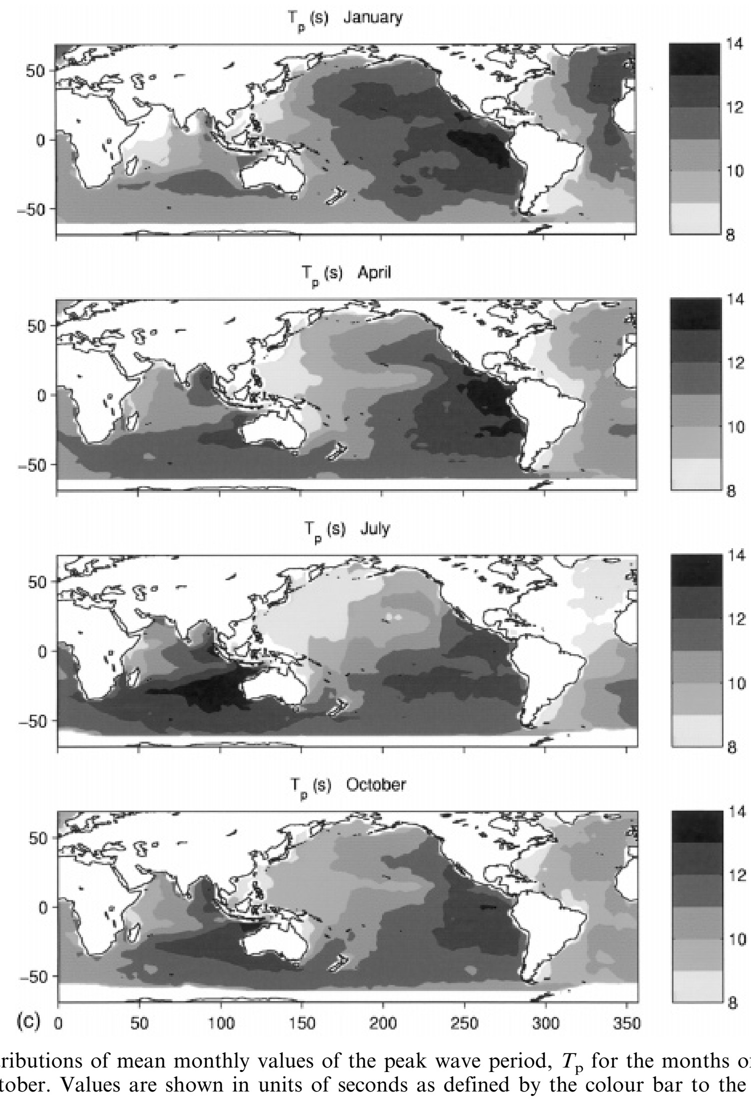

Figure 1(c). Global distributions of mean monthly values of the peak wave period, T_p for the months of January, April, July and October. Values are shown in units of seconds as defined by the colour bar to the right

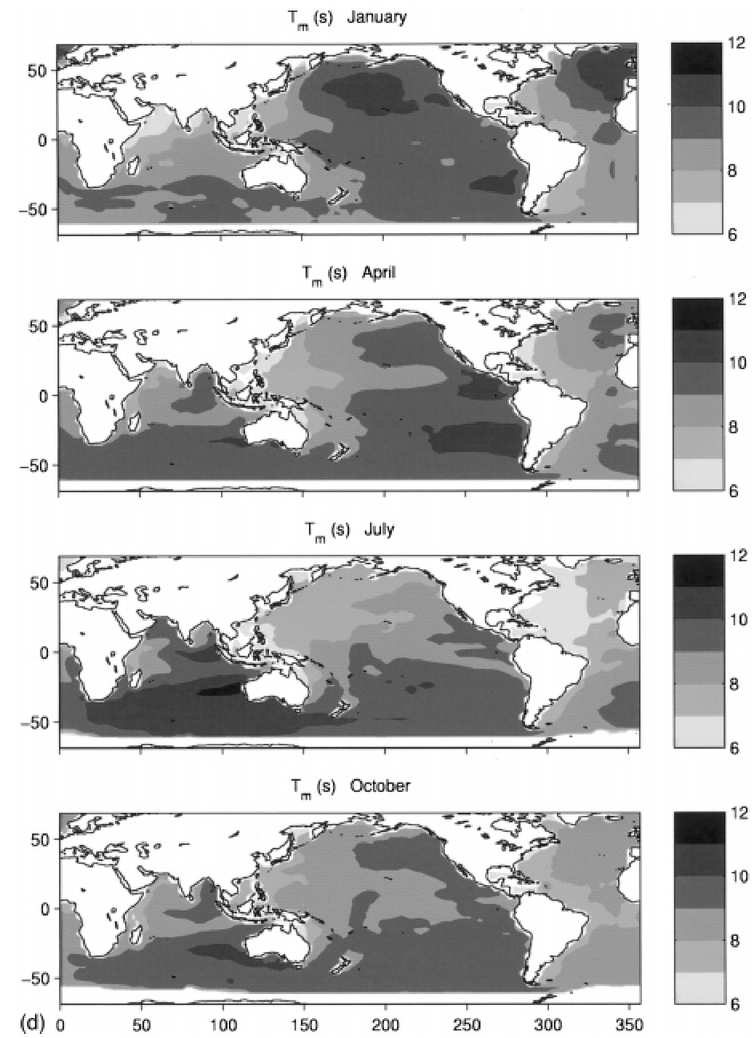

Figure 1(d). Global distributions of mean monthly values of the mean wave period, T_m for the months of January, April, July and October. Values are shown in units of seconds as defined by the colour bar to the right

4.3. *Swell propagation*

Figure 1(c) clearly shows that very long waves (large T_p) exist off the west coasts of the Americas as well as Australia. The region off Australia peaks with the onset of the high wave activity which occurs in the Southern Ocean during the Southern Hemisphere winter. These long waves appear to correspond to swell which was originally generated in the intense wave region of the Southern Ocean between Australia and South Africa and has propagated north-east along the great-circle path from this area. This assumption is confirmed by the θ_w fields shown in Figure 1(e), which show waves in the area propagating from the south-west.

The region off the west coast of the Americas is less easily explained as it is potentially affected by swell propagating from both the North Pacific and the Southern Ocean. Examination of the mean wind directions (Figure 1(f)), shows that both of these west coast regions (Australia and Americas) are predominately in the easterly trade wind belts with relatively consistent east to south-east winds all year round. Mean wave directions, however, diverge from the local wind directions considerably. In both areas the mean wave directions are from the south or south-west, consistent with the assumption that it is predominately controlled by Southern Ocean swell. Waves in the region off Western Australia are predominately from the south with the direction turning more to the south-west as the Southern Ocean wave climate increases in magnitude during the Southern Hemisphere winter. Indeed, a characteristic of the Indian Ocean is the dominant role Southern Ocean swell plays throughout the entire basin. The dominance of the Southern Ocean swell declines during the Southern Ocean summer, but still continues as far north as the Indonesia islands (Figure 1(e)). For the rest of the year, the predominately southern wave direction exists throughout the full basin.

The situation in the Pacific is more complex as a result of the possible propagation of swell from high latitudes of both hemispheres. During January (Figure 1(e)) a clear 'front' can be seen from New Zealand to Central America. This front marks the boundary between the domains of dominance of swell from each of the hemispheres. North of this front the mean wave direction is from the north, consistent with swell propagating from the intense storms of the North Pacific winter. South of the front, the mean wave direction is from the south-west consistent with the propagation of Southern Ocean swell. By April, this front has moved further north to lie between Mexico and New Guinea. This occurs as a result of the seasonal strengthening of the Southern Ocean wave climate together with the similar weakening of the North Pacific system. This process continues, and by July the front has almost completely disappeared,

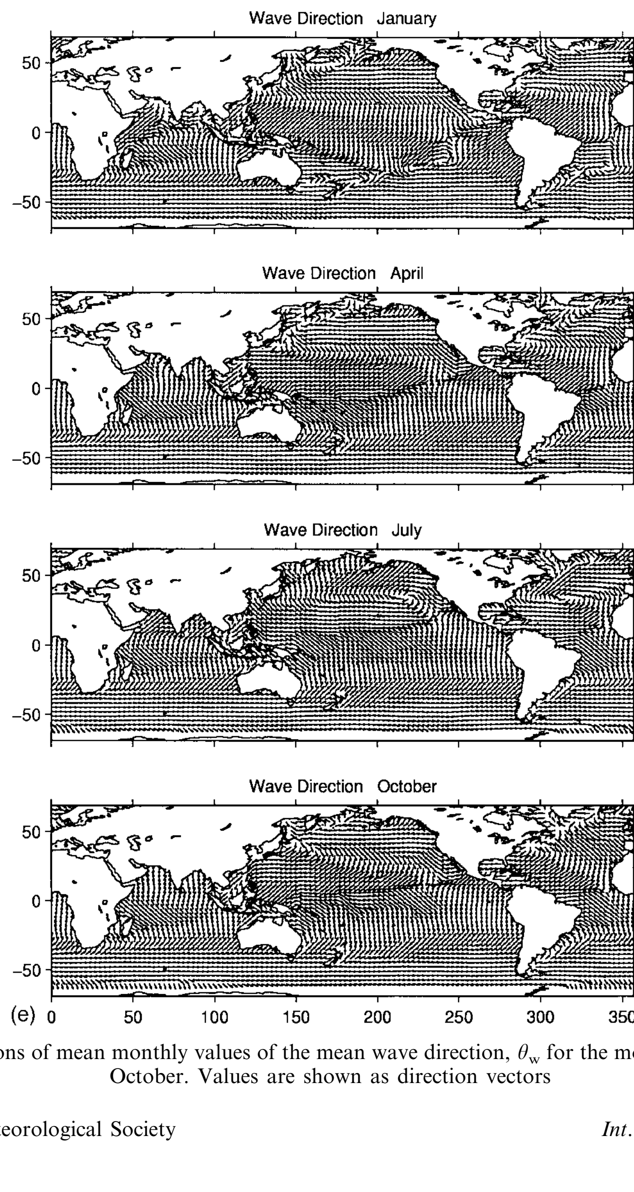

Figure 1(e). Global distributions of mean monthly values of the mean wave direction, θ_w for the months of January, April, July and October. Values are shown as direction vectors

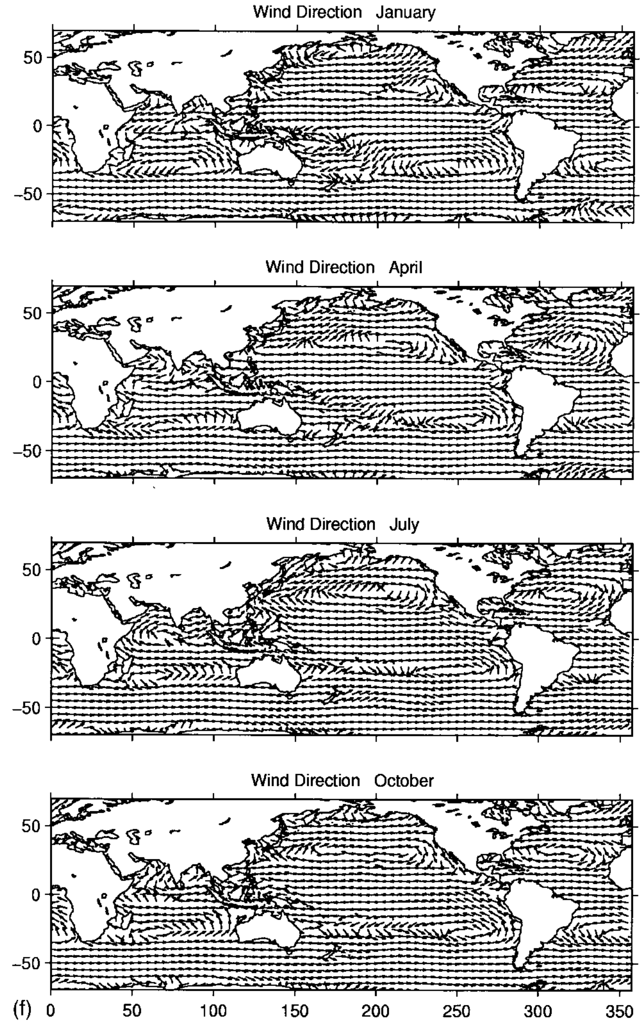

Figure 1(f). Global distributions of mean monthly values of the mean wind direction, for the months of January, April, July and October. Values are shown as direction vectors

the Southern Ocean swell system dominating the entire Pacific basin. By October, the North Pacific wave field has again strengthened, the swell 'front' moving south in response, to lie approximately along the equator.

As a result of the process described above, the west coast of the Americas is influenced by long period swell propagating from both hemispheres. This is particularly so in Central America where the swell 'front' seasonally migrates along the coast.

As with the other oceanic basins, the longest waves in the Atlantic Ocean occur along the coasts of Western Europe and West Africa (Figure 1(c)). A swell front, marking the extent of swell propagation from the high latitudes of each hemisphere is also visible (Figure 1(e)). This front is less distinct than in the Pacific, probably as a result of the weaker Southern Ocean generation region for the Atlantic and the fact that the propagation distances are significantly shorter than in the Pacific. The relatively narrow geometry of the Atlantic also restricts propagation of Southern Ocean swell into the Northern Hemisphere. The swell front does not migrate north of the equator, in marked contrast to the Pacific.

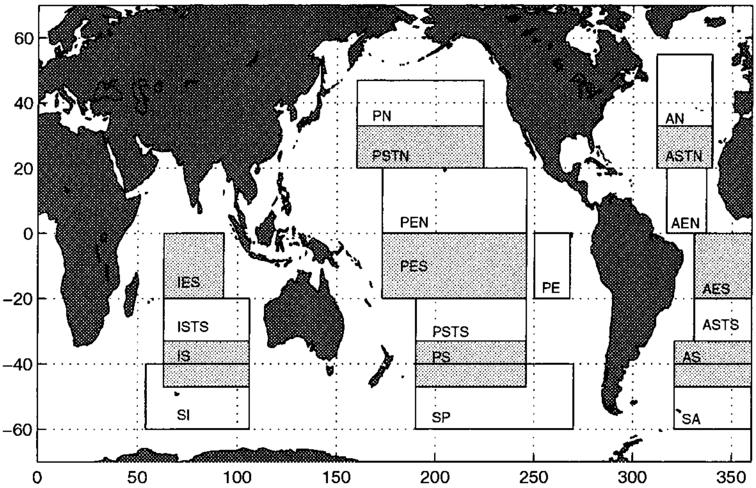

Figure 2. Regions of the globe used to form averages shown in Figure 3(a)–(f). The identifying symbols are shown for each region (PN, PSTN etc.). The details of the latitude and longitude extent of each region appear in Table I

5. REGIONAL VARIATIONS OF CLIMATE

In an effort to compare the ocean climate between regions, a number of representative regional zones have been selected. These zones are shown in Figure 2 and their characteristics documented in Table I. Regions with similar zonal extent have been selected for each major oceanic basin to facilitate intercomparison. The various ocean wind and wave parameters mentioned earlier have been averaged over each of these zones and are compared in the time series plots of monthly mean values shown in Figures 3(a)–(f). Although the averaging process filters out many local events, it provides a useful method of investigating regional trends in a relatively succinct form. The wave climate in each of these zones is considered below.

Table I. Geographical extent of regions for which wave conditions appearing in Figure 3(a)–(f) have been averaged

Region	Symbol	Longitude extent	Latitude extent
North Pacific	PN	160–224°E	33–47°N
North Subtropical Pacific	PSTN	160–224°E	20–33°N
Equatorial Pacific (north)	PEN	173–246°E	0°–20°N
Equatorial Pacific (south)	PES	173–246°E	20°S–0°
South Subtropical Pacific	PSTS	190–246°E	33–20°S
South Pacific	PS	190–246°E	47–33°S
Southern Ocean (Pacific)	SP	190–270°E	60–40°S
Eastern Pacific	PE	250–268°E	20°S–0°
North Atlantic	AN	312–340°E	33–55°N
North Subtropical Atlantic	ASTN	312–340°E	20–33°N
Equatorial Atlantic (north)	AEN	317–337°E	0°–20°N
Equatorial Atlantic (south)	AES	331–360°E	20°S–0°
South Subtropical Atlantic	ASTS	331–360°E	33–20°S
South Atlantic	AS	321–360°E	47–33°S
Southern Ocean (Atlantic)	SA	321–360°E	60–40°S
Equatorial Indian (south)	IES	63–93°E	20–0°
South Subtropical Indian	ISTS	63–106°E	33–20°S
South Indian	IS	63–106°E	47–33°S
Southern Ocean (Indian)	SI	54–106°E	60–40°S

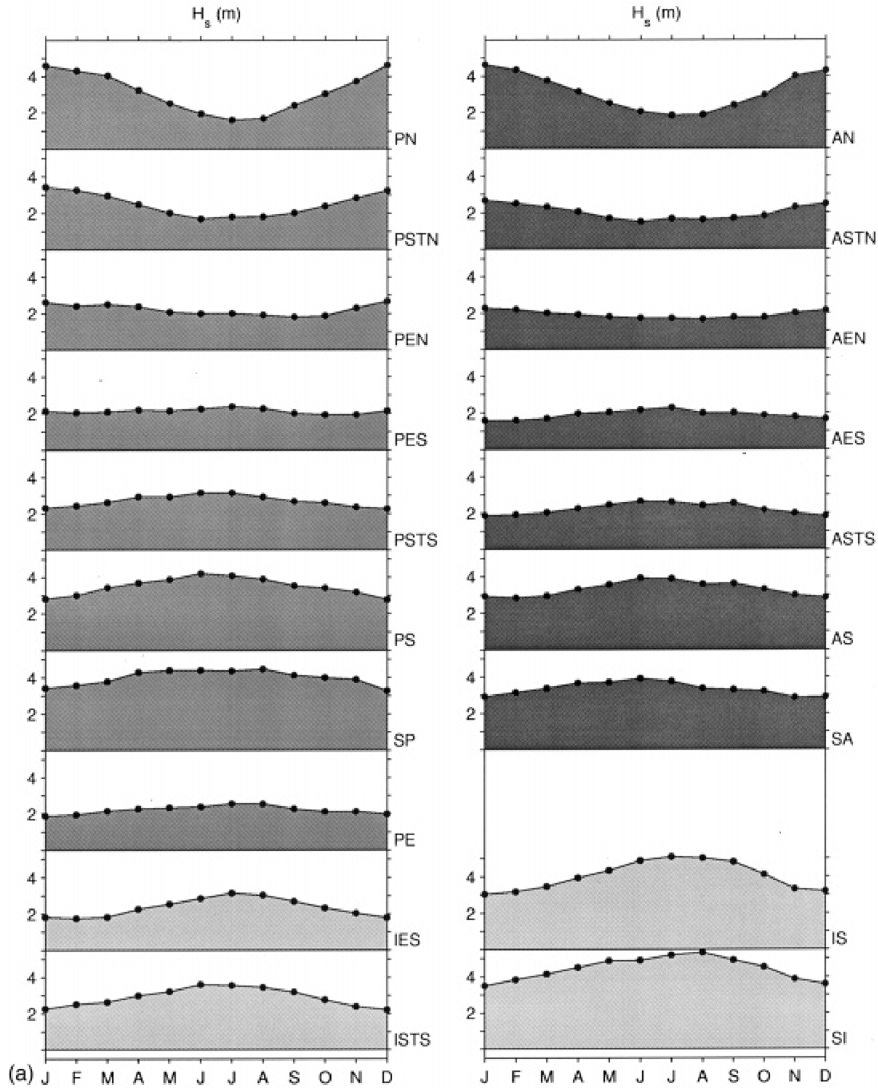

Figure 3(a). Seasonal variability of the significant wave height, H_s for the regions shown in Figure 2. The units used on the vertical axis are meters. The identifier for each region is shown to the right of the plot

5.1. Northern latitudes

The North Atlantic (AN) and North Pacific (PN) are characterised by strong seasonal trends for both H_s and U_{10}. The time series for both H_s and U_{10} are remarkably similar for the two basins (Figures 3(a) and 3(b)). The North Atlantic has slightly stronger winds and hence greater waves in summer than the North Pacific. Winter conditions are, however, almost identical for these two zones. Peak wave periods, T_p are also very similar with summer values in the North Pacific being slightly longer than the North Atlantic (Figure 3(c)). This result, taken together with the H_s and U_{10} results indicates that the North Atlantic has a higher incidence of storms in summer than the North Pacific. Hence, the wave field in the North Pacific is more swell-dominated in summer, being less influenced by local storm events. The θ_w is also more southerly during summer than the North Atlantic, indicating a greater penetration of Southern Ocean swell into the North Pacific than the North Atlantic (Figure 3(e)). This is not surprising, as the Pacific basin is significantly wider than the Atlantic, enabling a clearer great-circle path for swell propagation from the south.

5.2. Northern subtropics

The seasonal variation in the northern subtropical regions of both the Pacific (PSTN) and the Atlantic (ASTN) are reduced compared to the respective zones to the north. These two oceanic basins have similar climates at these subtropical latitudes, although the Pacific has more severe winter conditions than the Atlantic. As with regions further to the north, the Pacific has higher values of T_p during summer, consistent with the greater penetration of Southern Ocean swell into the region (see θ_w values in Figure 3(e)). These subtropical regions are characterised by year-round easterly trade winds (Figure 3(f)). Wave directions (Figure 3(e)), however, deviate considerably from the local wind direction. In the Pacific, the waves are from the north-west during winter moving to the south-east during summer. This reflects the influence of the swell generation regions of the North Pacific and Southern Oceans. In contrast, wave directions in the Atlantic are more northerly during winter. This occurs because this basin is much narrower than the Pacific, and hence propagation from a more westerly direction (as in the Pacific) is not possible. As in the Pacific, the wave direction moves more to the south in summer, but this effect is less pronounced in the Atlantic.

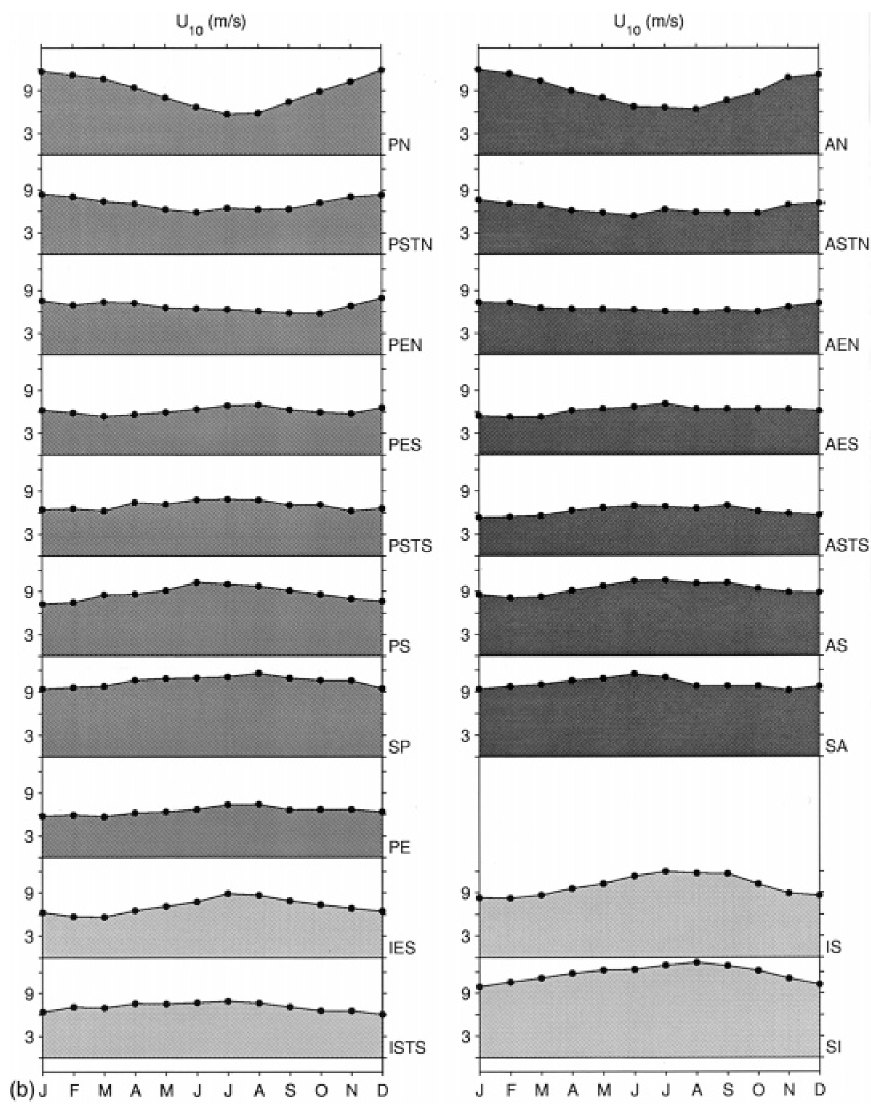

Figure 3(b). Seasonal variability of the wind speed, U_{10} for the regions shown in Figure 2. The units used on the vertical axis are m s^{-1}. The identifier for each region is shown to the right of the plot

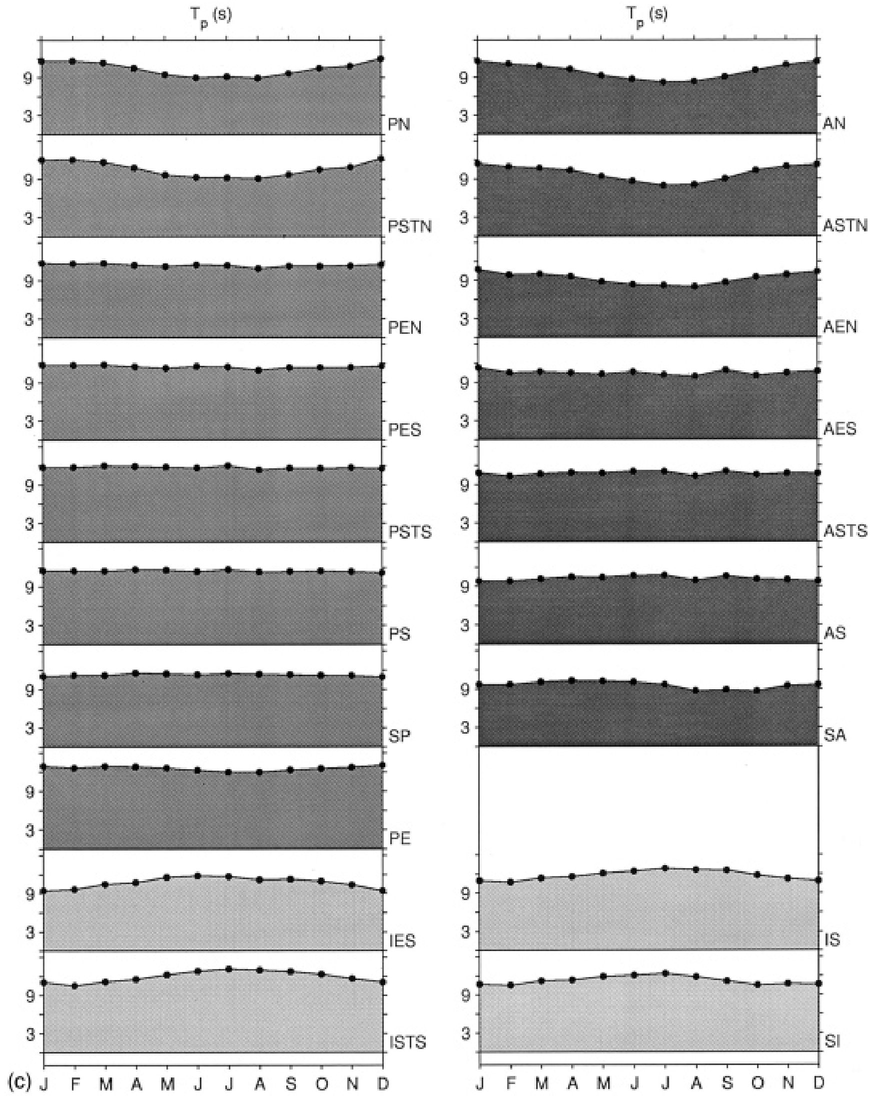

Figure 3(c). Seasonal variability of the peak wave period, T_p for the regions shown in Figure 2. The units used on the vertical axis are seconds. The identifier for each region is shown to the right of the plot

5.3. Equatorial regions

Equatorial regions of both the Pacific and Atlantic (PEN, PES, AEN. AES) are characterised by little seasonal variability either of U_{10} or H_s. In contrast, the Indian Ocean (IES) has a much greater seasonal variability with significantly higher values of both U_{10} and H_s in the Southern Hemisphere winter than in summer. Similarly, there is little seasonal variation in T_p in either the Pacific or Atlantic. The Indian Ocean, however, has a clear increase in the magnitude of T_p during the Southern Hemisphere winter (Figure 3(c)). All equatorial regions are characterised by weak year-round easterly winds (Figure 3(f)). The wave fields are, however, dominated by high latitude swell. In the Pacific, equatorial regions (both north and south) are dominated by northerly swell during the Northern Hemisphere winter and southern swell during the Southern Hemisphere winter. This same trend is seen in the northern equatorial regions of the Atlantic (AEN). Southern equatorial regions of the Atlantic (AES) have a relatively constant year-round south-easterly wave direction. This indicates that the basin geometry largely prevents North

Atlantic swell penetrating into the Southern Hemisphere. The dominance of the intense wave regions of the Southern Ocean between Australia and South Africa are clearly seen in the Indian Ocean Equatorial regions. The wave direction in this region is from the south throughout the year.

5.4. Southern subtropics

The Indian Ocean southern subtropical region (ISTS) has higher winter wave conditions than the corresponding Pacific region, followed by the Atlantic. This is partly as a result of the magnitude of Southern Ocean swell entering each region, but more directly as a result of corresponding differences in the wind conditions in each basin. In contrast, the Indian Ocean has the lowest values of wave height of the three basins in summer. The Pacific and Atlantic basins are similar during summer, with the Pacific yielding slightly higher values of H_s. Again, these trends largely reflect wind speed variations for the respective basins. The Pacific and Atlantic southern subtropical regions have little seasonal variability of

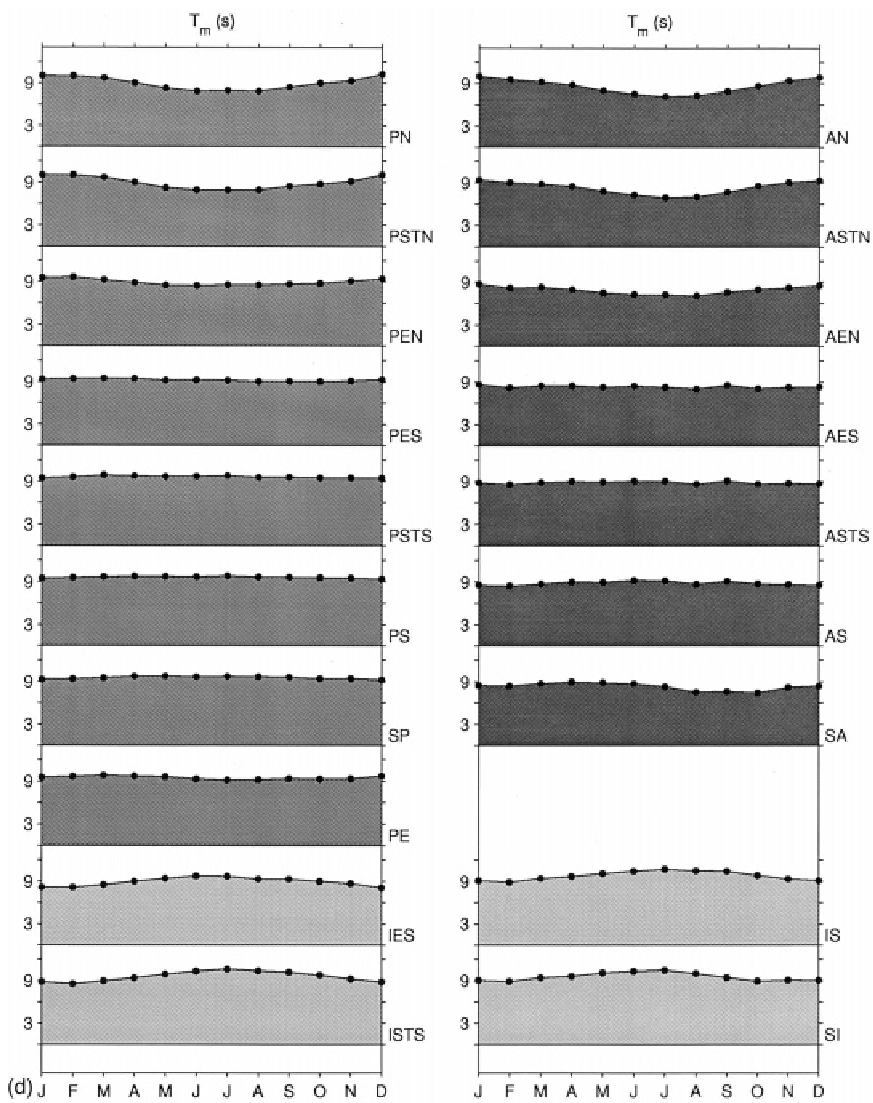

Figure 3(d). Seasonal variability of the mean wave period, T_m for the regions shown in Figure 2. The units used on the vertical axis are seconds. The identifier for each region is shown to the right of the plot

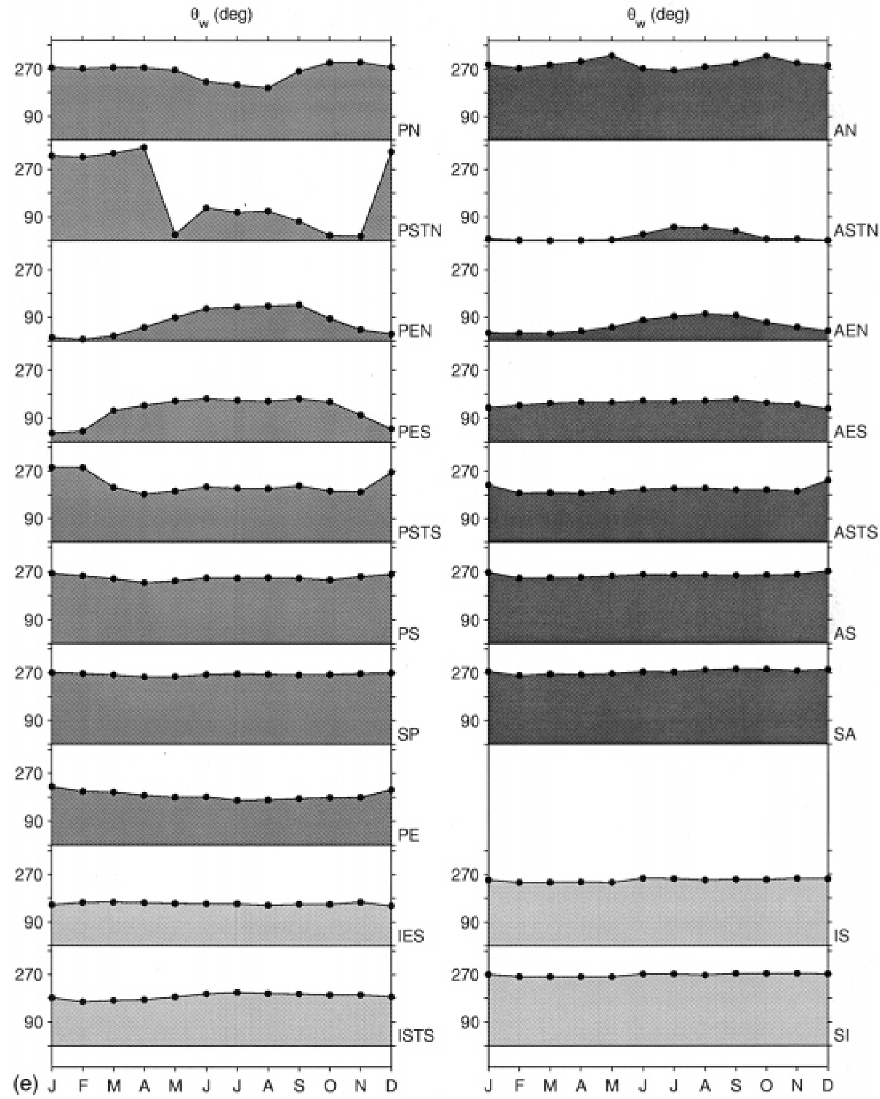

Figure 3(e). Seasonal variability of the mean wave direction, θ_w for the regions shown in Figure 2. The units used on the vertical axis are degrees. The identifier for each region is shown to the right of the plot

T_p (Figure 3(c)). The Indian Ocean, however, clearly shows longer waves during the Southern Hemisphere winter. This reflects the significant penetration of Southern Ocean swell into the Indian Ocean, as noted earlier. Both the Pacific and Atlantic southern subtropical regions experience winds which are westerly during the Southern Hemisphere winter and easterly during the summer (Figure 3(f)). In contrast, wave directions are largely southerly in both basins, as a result of Southern Ocean swell (Figure 3(e)). There is, however, some evidence of more northerly wave conditions in the Pacific during the Southern Hemisphere summer as a result of Northern Hemisphere swell. The Indian Ocean has largely uniform easterly winds. although the wave direction is dominated year round by southerly swell.

5.5. Southern latitudes

As noted in Figure 1(a)–(f), the most severe wave conditions occur in the Southern Ocean between Australia and South Africa (SI) (Figure 3(a)). This is largely as a result of the correspondingly strong winds in the region. In comparison to similar regions in the Northern Hemisphere, there is less seasonal variability in wind speed and hence wave height in the Southern Hemisphere than in the north (compare PN and PS or AN and AS). There is also no evidence of Northern Hemisphere penetration of swell into these southern latitudes (in contrast to that seen in the North Pacific). Both wind and wave conditions are year-round westerly.

5.6. Eastern Pacific

As noted in Figure 1 (a)–(f), the area of the globe where the longest period waves are found is in the Eastern Pacific (PE). This area is characterised by relatively light, year-round easterly winds. The waves are, however, largely from the south with some evidence of Northern Hemisphere swell during the Southern Hemisphere summer. There is little variation in values of T_p for this region, which are in excess of 12 s throughout the year.

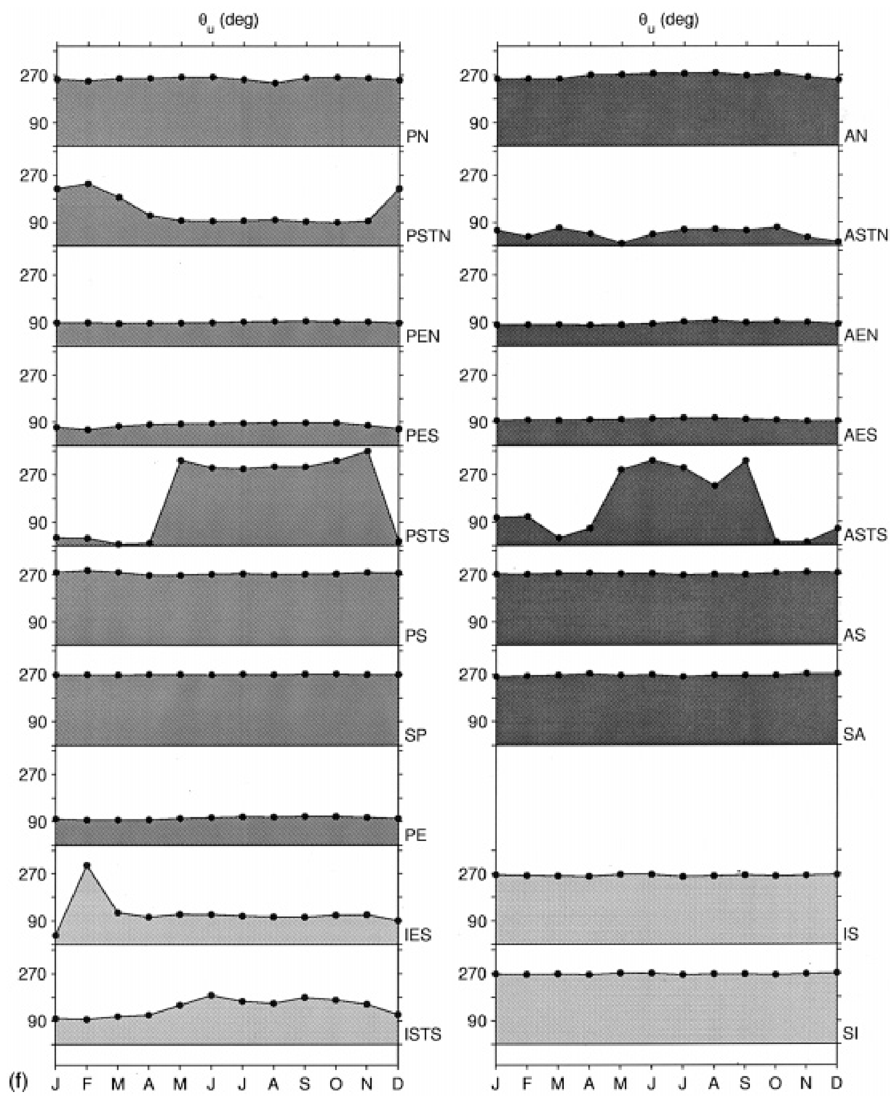

Figure 3(f). Seasonal variability of the mean wind direction, θ_u for the regions shown in Figure 2. The units used on the vertical axis are degrees. The identifier for each region is shown to the right of the plot

5.7. Arabian Sea

In addition to the basin-scale variations in wave climate noted above, very localised variations also occur. The clearest example of this occurs in the Arabian Sea. This area lies in the tropics and, as with most other tropical areas is generally calm. During July–August, however, a strong south-westerly jet develops close to the African coast (Figures 1(b) and 1(f)). This jet is associated with the Asian summer monsoon. The result is localised mean monthly values of H_s as large as 5 m and U_{10} values of 15 m s^{-1}. The existence of such conditions has been confirmed by Anderson and Prell (1992).

6. CONCLUSIONS

By combining satellite altimeter data and model results a composite ocean climate data set spanning 10 years has been compiled. This data set includes information on: significant wave height; wave period and direction; as well as wind speed and direction. The temporal extent and spatial coverage has enabled a global ocean wave climatology to be developed. This climatology shows the seasonal variability of ocean wind and wave conditions on a $2° \times 2°$ resolution grid.

Numerous features of the global wave climate have been investigated with the data set. The most striking feature of the global wave height field is the zonal variation. The highest waves exist at the high latitudes with the wave climate progressively moderating with reducing distance from the equator. This trend is also generally seen in the wind field distribution. Clear local zonal maxima, however, exist in the trade wind belts. Similar maxima do not occur in the wave fields as a result of the dispersive nature of waves. Waves are not purely local. Once generated, they propagate large distances, thus masking local generation events.

The ubiquitous nature of swell is clearly seen in the data. In particular, swell generated in the intense wind regions of the Southern Ocean has significant impact on much of the world's oceans. Southern Ocean swell penetrates the full Indian Ocean and during the Southern Hemisphere winter can even penetrate into the North Pacific. As a result of the narrower geometry of the Atlantic Ocean, however, Southern Ocean swell does not appear to influence conditions in the North Atlantic.

Although the data set is comprehensive, the 10-year duration is still probably too short to provide reliable information on extreme wave conditions. However, with time, the potential exists for the study of extremes.

REFERENCES

Anderson, D.M. and Prell, W.L. 1992. 'The structure of the southwest monsoon winds over the Arabian Sea during the late Quaternary: Observations, simulations, and marine geologic evidence', *J. Geophys. Res.*, **97**(10), C15, 481–487.

Alpers, W. 1983. 'Monte Carlo simulations for studying the relationship between ocean wave and synthetic aperture radar image spectra', *J. Geophys. Res.*, **88**, 1745–1759.

Alpers, W.R. and Rufenach, C.L. 1979. 'The effect of orbital motions on synthetic aperture radar imagery of ocean waves', *IEEE Trans. Antennas Propag.*, **AP-27**, 685–690.

Alpers, W.R., Ross, D.B. and Rufenach, C.L. 1981. 'On the detectability of ocean surface waves by real and synthetic aperture radar', *J. Geophys. Res.*, **86**, 6481–6498.

Alpers, W. and Brüning, C. 1986. 'On the relative importance of motion related contributions to the SAR imaging mechanism of ocean surface waves', *IEEE Trans. Geosci. Remote Sens.*, **GE-24**, 873–885.

Carter, D.J.T., Foale, S. and Webb, D.J. 1991. 'Variation in global wave climate throughout the year', *Int. J. Remote Sensing*, **12**(8), 1687–1697.

Challenor, P.G., Foale, S. and Webb, D.J. 1990. 'Seasonal changes in the global wave climate measured by the Geosat altimeter', *Int. J. Remote Sensing*, **11**(12), 2205–2213.

Chelton, D.B. and Wentz, F.J. 1986. 'Further development of an improved altimeter wind speed algorithm', *J. Geophys. Res.*, **91**, 14250–14260.

Chelton, D.B., Hussey, K.J. and Parke, M.E. 1981. 'Global satellite measurements of water vapor, wind speed and wave height', *Nature*, **294**, 529–532.

Cotton, P.D. and Carter, D.J.T. 1994. 'Cross calibration of TOPEX, ERS1, and Geosat wave heights', *J. Geophys. Res.*, **99**, 25025–25033.

Dobson, E.B. and Monaldo, F.M. 1996. 'Radar altimeter wave height measurements', in Ikeda, M. and Dobson, F. (eds), *Remote Sensing Techniques for Oceanographers*, CRC Press, New York.

Gulev, S.K., Cotton, D. and Sterl, A. 1998. 'Intercomparison of the North Atlantic wave climate from voluntary observing ships, satellite data and modelling', *Phys. Chem. Earth*, **23**.

Hasselmann, K., Raney, R.K., Plant, W.J., Alpers, W., Schuchman, R.A., Lyzenga, D.R., Rutenach, C.L. and Tucker, M.J. 1985. 'Theory of Synthetic Aperture Radar ocean imaging—A MARSEN view', *J. Geophys. Res.*, **90**, 4659–4686.

Hasselmann, S., Brüning, C. and Hasselmann, K. 1996. 'An improved algorithm for the retrieval of ocean wave spectra from synthetic aperture radar image spectra', *J. Geophys. Res.*, **101**, 16615–16629.

Hogben, N. and Lumb, P. 1967. *Ocean Wave Statistics*, Ministry of Technology, HMSO, London, 263 pp.

Hogben, N., Dacunha, N.M.C. and Oliver, G.F. 1986. *Global Wave Statistics*, Unwin Brothers, London, 661 pp.

Hollinger, J. 1991. *DMSP SSM/I calibration/validation*, Final rep. I & II, Naval Research Lab., Washington, 453 pp.

Janssen, P.A.E.M., Hansen, B. and Bidlot, J. 1996. *Verification of the ECMWF Wave Forecasting System Against Buoy and Altimeter Data*, European Centre for Medium-Range Weather Forecasts, Tech. Memor. No. 229.

Komen, G.J., Cavaleri, L., Donelan, M., Hasselmann, K., Hasselmann, S. and Janssen, P.A.E.M. 1994. *Dynamics and Modelling of Ocean Waves*, Cambridge Univ. Press, 532 pp.

Mognard, N.M., Campbell, W.J., Cheney, R.E. and Marsh, J.G. 1983. 'Southern Ocean mean monthly wave and surface winds for winter 1978 by SEASAT radar altimeter', *J. Geophys. Res.*, **88**, 1736–1744.

Raney, R.K. 1981. 'Wave orbital velocity, fade, and SAR response to azimuth waves', *IEEE J. Oceanic Eng.*, **OK-6**, 140–146.

Romeiser, R. 1993. 'Global validation of the wave model WAM over a one-year period using GEOSAT wave height data', *J. Geophys. Res.*, **98**, 4713–4726.

Sterl, A., Komen, G.J. and Cotton, P.D. 1998. 'Fifteen years of global wave hindcasts using winds from the European Centre for Medium-Range Weather Forecasts reanalysis: Validating the reanalyzed winds and assessing the wave climate', *J. Geophys. Res.*, **103**, 5477–5492.

Tournadre, J. and Ezraty, R. 1990. 'Local climatology of wind and sea state by means of satellite radar altimeter measurements', *J. Geophys. Res.*, **95**, 18255–18268.

Witter, D.L. and Chelton, D.B. 1991. 'A Geosat altimeter wind speed algorithm and a method for altimeter wind speed algorithm development', *J. Geophys. Res.*, **96**, 8853–8860.

Young, I.R. 1993. 'An estimate of the Geosat altimeter wind speed algorithm at high wind speeds', *J. Geophys. Res.*, **98**, 20275–20285.

Young, I.R. 1994. 'Global ocean wave statistics obtained from satellite observations', *Appl. Ocean Res.*, **16**, 235–248.

Young, I.R. 1998. 'An intercomparison of GEOSAT, TOPEX and ERS1 measurements of wind speed and wave height', *Ocean Eng.* (in press).

Young, I.R. and Holland, G.J. 1996. *Atlas of the Oceans: Wind and Wave Climate*, Pergamon Press, 241 pp.

